COBEM 99
XV Congresso Brasileiro de Engenharia Mecânica
15th Brazilian Congress of Mechanical Engineering
22 - 26 de Novembro de 1999 / November 22 - 26, 1999 Águas de Lindóia, São Paulo,

# A FRAMEWORK TO CORRELATE EFFECTS OF CONSTRAINT LOSS AND DUCTILE TEARING ON FRACTURE TOUGHNESS – PART II : FRACTURE UNDER SMALL SCALE YIELDING CONDITIONS

**Claudio Ruggieri**
**Euclydes Trovato Neto**
Department of Naval Architecture and Ocean Engineering, University of São Paulo
São Paulo, SP 05508–900, E-mail: cruggi@usp.br, Brazil

***Abstract*** *– The characterization of fracture resistance using small scale yielding (SSY) solutions coupled with a micromechanics model for cleavage fracture based upon the Weibull stress is the focus of this paper. A computational model employing a modified boundary layer (MBL) formulation is employed to generate numerical solutions for the crack-tip stress fields of cracked body with well-contained plasticity near the crack tip. One key feature of our investigation is the generation of crack-tip fields differing in stress triaxiality by varying the non-singular stress, T, parallel to the crack plane. This introduces the notion of reference fields to provide a measure of constraint loss when large scale yielding (LSY) effects arise in finite bodies. Another feature of the present investigation is the realistic modeling of ductile tearing and its implications on the (macroscopic) fracture resistance behavior. The Weibull stress trajectories under small scale yielding analyses with varying levels of T-stress provide valuable insight about the effects of crack-tip constraint and ductile tearing on fracture resistance.*

**Key words**: *cleavage fracture, statistical effects, weakest link, local approach, Weibull stress*

## 1. INTRODUCTION

In Part I of this article [1], a micromechanics (probabilistic) methodology provides the basis for establishing a relationship between the microregime of fracture and macroscopic crack driving forces (such as the $J$-integral) by introducing the Weibull stress ($\sigma_w$) [2] as a probabilistic fracture parameter. A key feature in this *predictive* framework is that the Weibull stress incorporates *both* the effects of stressed volume ahead of a macroscopic crack and the potentially strong changes in the character of the near-tip stress fields due to constraint loss and ductile crack extension. Unstable crack propagation occurs at a critical value of $\sigma_w$ which may be attained prior to or following some amount of stable, ductile crack extension; the outcome being determined by the specimen geometry, loading mode (tension *vs.* bending), material flow properties and micro-scale tearing resistance. Here, the critical Weibull stress represents a property of the material, possibly dependent on temperature, but invariant of loading history. Under increased remote loading (as measured by $J$), differences in evolution of the Weibull stress reflects the stress history at material points ahead of the crack tip. When implemented in a finite element code, the computational model predicts the evolution of the Weibull stress with crack-tip stress triaxiality and ductile tearing.

The characterization of fracture resistance using small scale yielding (SSY) solutions coupled with a micromechanics model for cleavage fracture based upon the Weibull stress is the focus of this paper. A computational model employing a modified boundary layer (MBL) formulation [15] is employed to generate numerical solutions for the crack-tip stress fields of cracked body with well-contained plasticity near the crack tip. One key feature of our investigation is the generation of crack-tip fields differing in stress triaxiality by varying the non-singular stress, $T$, parallel to the crack plane [3]. This introduces the notion of reference fields to provide a measure of constraint loss when large scale yielding (LSY) effects arise in finite bodies [17]. Another central feature of the present investigation is the realistic modeling of ductile tearing and its implications on the (macroscopic) fracture resistance behavior. Here, a realistic modeling of ductile crack growth using the computational cell methodology [19-21,27] defines the evolution of near-tip stress fields during crack extension. A simplified form of the Gurson-Tvergaard (GT) [22, 23] constitutive model for dilatant plasticity serves to predict microscopic void growth within a layer of cells defined over the crack plane. The Weibull stress trajectories under small scale yielding analyses with varying levels of $T$-stress provide valuable insight about the effects of crack-tip constraint and ductile tearing on fracture resistance.

## 2. MICROMECHANICS MODELING OF CLEAVAGE FRACTURE

### 2.1 The Weibull Stress for Stationary and Growing Cracks

Following the development of a local approach (micromechanics model employing weakest link philosophy and statistics of microcracks) applicable for cleavage fracture described in Part I [1], the Weibull stress ($\sigma_w$) [2] emerges as a probabilistic fracture parameter given by integration of the (local) principal stress over the fracture process zone in the form [4-7]

$$\sigma_w = \left[ \frac{1}{V_0} \int_{\Omega} {\sigma_1}^m d\Omega \right]^{1/m} , \tag{1}$$

where $\sigma_1$ is the maximum principal stress, $\Omega$ denotes the volume of the (near-tip) fracture process zone defined by the loci $\sigma_1 \geq \lambda\sigma_0$ with $\lambda \approx 2$, and parameter $m$ (the Weibull moduluS) define the microcrack distribution.

When small amounts of ductile crack growth precede unstable crack propagation by a cleavage mechanism, the stress history of material points within the process zone for cleavage fracture is altered thereby affecting directly the evolution of the Weibull stress. Crack growth elevates the near-tip stress triaxiality, particularly for low constraint configurations, and enlarges the fracture process zone [24,25]. Thus, a convenient form of the Weibull stress for an extending crack is obtained by integrating the principal stresses over the *active* volume of the fracture process zone which moves forward with the advancing tip [4-6] as

$$\sigma_w = \left[ \frac{1}{V_0} \int_{\Omega^*} {\sigma_1}^m d\Omega^* \right]^{1/m} , \tag{2}$$

where $\Omega^*$ denotes the volume of the active fracture process zone, $\sigma_1 \geq \lambda\sigma_0$ , which moves forward with the advancing tip. The proposed generalization of $\sigma_w$ to include ductile tearing maintains the relative simplicity of computations while, at the same time, fully incorporating the effects of alterations in the stress field ahead of the crack tip.

### 2.2 3-D Modeling of Ductile Crack Growth Using Computational Cells

A central feature of the present work is the realistic modeling of ductile tearing by void growth using the *computational cell* methodology [19-21,27] illustrated in Fig. 1(a). Void growth re-

mains confined to a layer of material symmetrically located about the crack plane and having thickness $D$, where $D$ is associated with the mean spacing of the larger, void initiating inclusions. This layer consists of cubical cell elements with dimension $D$ on each side; each cell contains a centered spherical cavity of initial volume fraction $f_0$ (the initial void volume divided by cell volume). Progressive void growth and subsequent macroscopic material softening in each cell are described with the Gurson-Tvergaard (GT) constitutive model for dilatant plasticity [22,23]. When $f$ in the cell incident on the current crack tip reaches a critical value, $f_e$, the computational procedures remove the cell thereby advancing the crack tip in discrete increments of the cell size. Figure 1(b) shows the typical, plane strain finite element representation of the computational cell model where symmetry about the crack plane requires elements of size $D/2$. Material outside the computational cells follows a conventional $J_2$ flow theory of plasticity and remains undamaged by void growth in the cells (see [27,18] for addtional details).

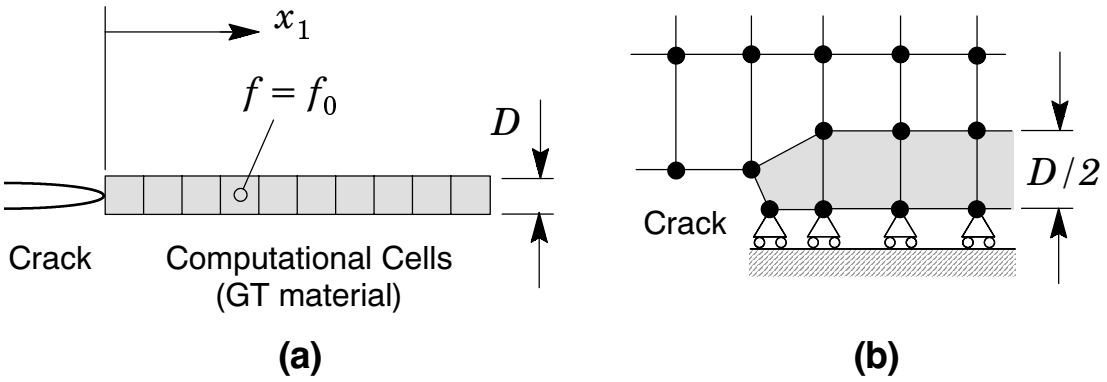


**Fig. 1.** Modeling of ductile tearing using computational cells.

## 3. COMPUTATIONAL MODEL AND MEASURE OF CONSTRAINT

### 3.1 Small Scale Yielding Model

The modified boundary layer model [15] simplifies the generation of numerical solutions for stationary cracks under well-defined SSY conditions with varying levels of constraint. Figure 2 shows the plane-strain finite element model for an infinite domain, single-ended crack problem with a initially blunted notch (finite root radius, $\rho = 2.5\mu$m); Mode I loading of the far field permits analysis using one-half of the domain as shown. With the plastic region limited to a small fraction of the domain radius, $R_p < R/20$, the general form of the asymptotic crack-tip stress fields well outside the plastic region is given by [26]

$$\sigma_{ij} = \frac{K_{\mathrm{I}}}{\sqrt{2\pi r}} f_{ij}(\theta) + T\delta_{1i}\delta_{1j} \tag{3}$$

where $K$ is the stress intensity factor, $f_{ij}(\theta)$ define the angular variations of in-plane stress components, and the non-singular term $T$ represents a tension (or compression) stress parallel to the crack. Numerical solutions for different levels of $T/\sigma_0$ are generated by imposing displacements of the elastic, Mode I singular field on the outer circular boundary ($r = R$) which encloses the crack

$$u(R,\theta) = K_{\mathrm{I}}\frac{1+\nu}{E}\sqrt{\frac{R}{2\pi}}\cos\left(\frac{\theta}{2}\right)(3 - 4\nu - \cos\theta) + T\frac{1-\nu^2}{E}R\cos\theta \tag{4}$$

$$v(R,\theta) = K_{\mathrm{I}}\frac{1+\nu}{E}\sqrt{\frac{R}{2\pi}}\sin\left(\frac{\theta}{2}\right)(3 - 4\nu - \cos\theta) - T\frac{\nu(1+\nu)}{E}R\sin\theta \tag{5}$$

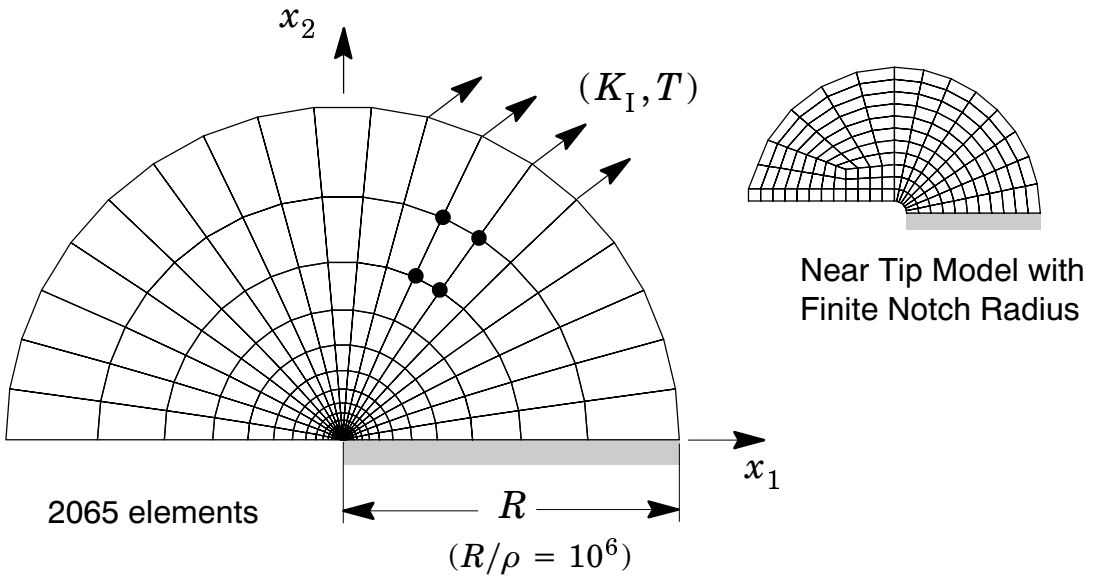


**Fig. 2.** SSY model with (K, T) fields imposed on boundary.

The uniaxial true stress ($\bar{\sigma}$)-logarithmic strain ($\epsilon$) response for the both the background and cell matrix materials follows a simple power-hardening model,

$$\frac{\epsilon}{\epsilon_0} = \frac{\bar{\sigma}}{\sigma_0} \quad \epsilon \le \epsilon_0 \; ; \qquad \frac{\epsilon}{\epsilon_0} = \left(\frac{\bar{\sigma}}{\sigma_0}\right)^n \quad \epsilon > \epsilon_0 \tag{6}$$

where $\sigma_0$ and $\epsilon_0$ are the reference (yield) stress and strain, and $n$ is the strain hardening exponent. Numerical solutions for the SSY boundary-layer model with non-zero $T$-stress are generated for material flow properties covering most structural and pressure vessel steels: $n = 5$ ($E/\sigma_0 = 800$), 10 ($E/\sigma_0 = 500$) and 20 ($E/\sigma_0 = 300$) with $E = 206$ GPa and $\nu = 0.3$; these ranges of properties also reflect the upward trend in yield stress with the decrease in strain hardening exponent characteristic of ferritic steels.

Finite element solutions are generated using the WARP3D code [13] which: (1) implements a Mises constitutive models in a finite-strain framework, (2) solves the equilibrium equations at each iteration using a linear pre-conditioned conjugate gradient (LPCG) method implemented within an element-by-element (EBE) software architecture, (3) evaluates the $J$-integral using a convenient domain integral procedure and (4) analyzes fracture models constructed with three-dimensional, 8-node tri-linear hexahedral elements.

## 3.2 Measure of Constraint Using the SSY Reference Fields

*Constraint* most generally refers to the evolving level of stress triaxiality ahead of the crack front under increased remote loading. A convenient approach to quantify the level of constraint in a finite cracked body utilizes a full "reference" fields constructed for small-scale yielding (SSY) conditions using large geometry changes (LCG) analysis; fields computed for the finite body are compared to SSY fields to define *relative* constraint differences. Such analyses enable construction of SSY fields for general material response and admit the option to include finite-strain (blunting) effects at the crack tip. Figures 3(a-d) provide key results to verify the existence of such fields under well-contained, limited scale plasticity for varying levels of applied $T$-stress. In the plots, distances all scale with $(K_I/\sigma_0)^2$ whereas the opening stresses are normalized by $\sigma_0$.

At very low remote loading for all levels of applied $T$-stress ($K_I$ = 20, 40 MPa $\sqrt{m}$), the near-tip stresses increase as the process of crack-tip blunting takes place. After the notch root radius increases to several times the initial radius $\rho$, a *steady state solution* develops so that the near-tip fields under SSY conditions are simply a continuous series of self-similar states. Additional analyses were also conducted for materials with $n = 5$ and $n = 20$; the crack-tip fields for these materials display essentially similar trends (to save space, they are not presented here). These plane-strain fields thus define a family of reference fields for stationary cracks where specified values for $K_I$ and $T$ uniquely define the elastic-plastic fields along the crack tip when a vanishingly small plastic zone encloses the tip. Consequently, the differences between the actual finite-body field and those of the comparison SSY field (having the applicable elastic $T$-stress), quantify the extent of large-scale yielding (LSY) effects or *loss of constraint* effects.

## 4. WEIBULL STRESS TRAJECTORIES UNDER SSY CONDITIONS

### 4.1 Stationary Cracks

Figures 4(a–d) provide key results to assess effects of constraint variations on macroscopic fracture toughness using the Weibull stress as a fracture parameter describing local conditions for material failure. In evaluating the Weibull stress, Eq. (1), under increasing $K_I$ levels, three values of the shape parameter are considered: $m = 10$, 20 and 30. In particular, $m \approx 20$ characterizes the distribution of Weibull stress at cleavage fracture for a nuclear pressure vessel steel (ASTM A508) [2]. These values of $m$ reflect different microcrack densities and thereby provide further insight into the fracture behavior for these materials.

Figures 4(a–c) show the variation of Weibull stress under increasing deformation for the three levels of hardening $n = 5$, 10, 20 each with $m = 20$, and for values of $T$-stress ranging from $-0.75 \leq T/\sigma_0 \leq 0.25$. For $T/\sigma_0 = 0$ and fixed strain hardening ($n = 10$), Figure 4(d) shows the variation of Weibull stress with increasing deformation for $m = 10$, 20 and 30. In these plots, $K_I^2/(\sigma_0^2 R)$ describes the far-field loading with the Weibull stress normalized by the yield stress, $\sigma_0$. The evolution of $\sigma_w$ as deformation progresses depends markedly on the degree of strain hardening and $T/\sigma_0$. Positive values of $T/\sigma_0$ have a small effect at all hardening levels. For all $T/\sigma_0$ levels, the Weibull stress for $n = 5$ increases steadily with deformation and remains well above the values for $n = 10$ and 20.

The most striking feature of these results, however, is the development of $\sigma_w$ with increasing deformation for negative values of $T$ in the materials with $n = 10$ and 20 (see Figs. 4(b,c)). The Weibull stress in these materials increases at a much lower rate with increasing deformation, especially for the low hardening material in the range $-0.75 \leq T/\sigma_0 \leq -0.5$. Under these conditions of severe constraint loss, there develops early in the loading a maximum value of $\sigma_w$ indicated by a marker ($\times$) on these curves. At higher remote loading but with continuing constraint loss, the Weibull stress decreases due to the lower near-tip stresses. In the post-peak regime, $\sigma_w$ as defined here cannot describe a realistic failure probability for the cracked body, which must continue to increase possibly by the intervention of ductile tearing as demonstrated in [4]. In contrast, $\sigma_w$ for $n = 5$ increases monotonically over the full range of deformation analyzed for all values of $T/\sigma_0$, i.e., the increased stresses provided by hardening more than offset the loss in stress triaxiality. These results demonstrate clearly the strong effect of constraint loss ($T/\sigma_0 < 0$) on the levels of $\sigma_w$ for moderate-to-low hardening materials. These trends remain relatively independent of the $m$-value adopted, as can be seen in Fig. 4(d). Here, $m$ simply scales the magnitude of Weibull stress after the early stages of loading in accordance with $\sigma_w = \beta_m K_I^{4/m}$ [9], where the proportionality constant, $\beta_m$, depends on $m$.

In summary, the micromechanics approach adopted admits the simple axiom that cleavage fracture occurs when the Weibull stress reaches a critical value, $\sigma_{wc}$, which is a material depen-

dent property. The analysis results shown in Fig. 4 demonstrate that attainment of $\sigma_{wc}$ for low constraint crack configurations occurs, if at all, only at much greater deformation levels ($K_I$) relative to high constraint configurations. Moreover, the combination of a low strain hardening material and a low constraint crack configuration may never generate $\sigma_w = \sigma_{wc}$, in which case cleavage fracture cannot occur unless some other event (e.g., ductile tearing) elevates the near-tip stresses.

## 4.2 Growing Cracks

The previous results demonstrate a significant reduction of the Weibull stress under low constraint conditions (negative $T$-stress) for low and moderately hardening materials. This section examines the potential for ductile tearing to counteract the effects of constraint loss and thus restore the Weibull stress to high constraint levels — such an outcome would aid in explaining the transition from a stable ductile tearing mode to a cleavage mode of fracture. To conserve space, we describe only key results computed for $m = 20$ (shape parameter) and $f_0 = 0.001$ (initial void fraction for the material). Similar trends and conclusions are drawn for other $m$ and $f_0$ values. For the strongly negative $T$-stress levels, these analyses typify cleavage fracture accompanied by small amounts of stable crack growth structural steels in low-constraint configurations. In the context of our computational cell model, values of $f_0$ (0.001–0.003) and cell sizes of $D \approx 200\mu$m characterize materials with moderate crack growth resistance [19-21].

Figures 5(a,c) show the computed crack growth resistance curves for materials having $n = 10$, 20 and $f_0 = 0.001$. $J$ is normalized by the cell size and flow stress ($D\sigma_0$) while $\Delta a$ is normalized by $D$. The cell with current porosity $f = 0.1$ defines the current crack tip location, and thus $\Delta a$ [19-21]. This "operational" definition locates the crack tip in the region behind the peak stress where stresses decrease rapidly, but ahead of the very highly damaged region, where the GT model does not accurately predict material response. Figures 5(b,d) present the dependency of $\sigma_w$, Eq. (2), on crack growth. For all levels of crack-tip constraint represented by $T/\sigma_0$, the Weibull stress increases monotonically with ductile extension (compare Figs. 5 (b,d) with the no-growth results in Figs. 4 (b,c)). The levels of $\sigma_w$ for the material with $n = 20$ remain consistently lower than the levels for the material with $n = 10$ at the same value of $T/\sigma_0$ and crack extension. These results clearly reflect the less severe near-tip stresses that develop for the $n = 20$ material and for low-constraint conditions. The computed $R$-curves at large growth reveal a different trend of lower toughness with higher strain hardening for all constraint levels.

In summary, these representative analyses demonstrate important features associated with the evolution of Weibull stress for a growing crack. The physical significance is this: ductile tearing increases the crack-tip driving force ($\sigma_w$) as deformation progresses particularly so for low-constraint configurations, which increases the likelihood of unstable crack propagation by cleavage. The trends shown here are consistent with those obtained in previous numerical analyses [28, 29] in that stable crack growth elevates the near-tip stresses and increases the volume of the cleavage fracture process zone. Since $\sigma_w$ explicitly incorporates the crack-tip stress field and the volume of the near-tip stressed material, it fully captures the governing features for cleavage fracture in growing cracks.

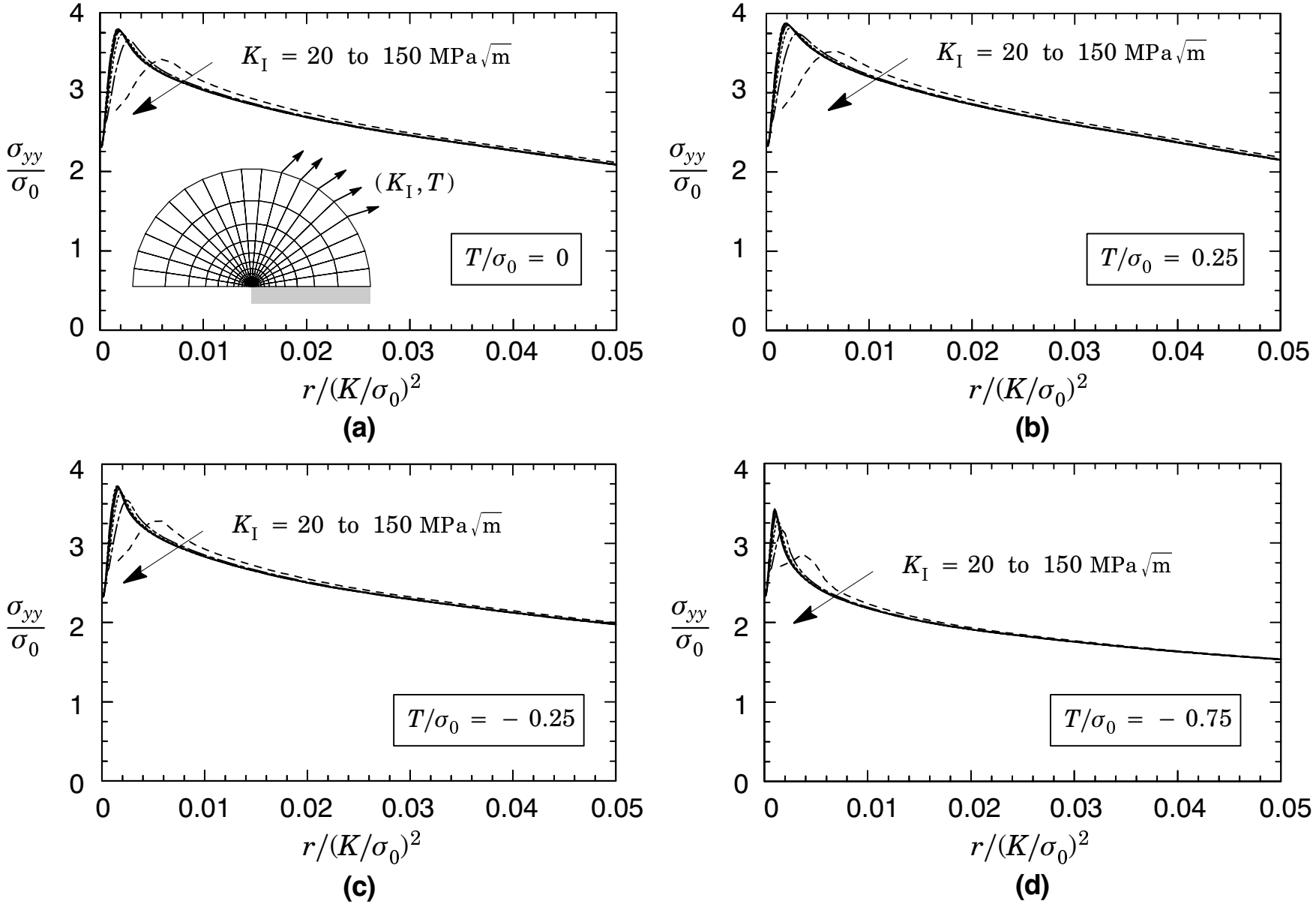


**Fig. 3.** Near-tip opening stresses under SSY conditions for n = 10, $E/\sigma_0 = 500$ and varying levels of applied T-stress. Plots are generated for load levels $K_I = 20$, 40, 60, 80, 100, 125 and 150 MPam$^{1/2}$.

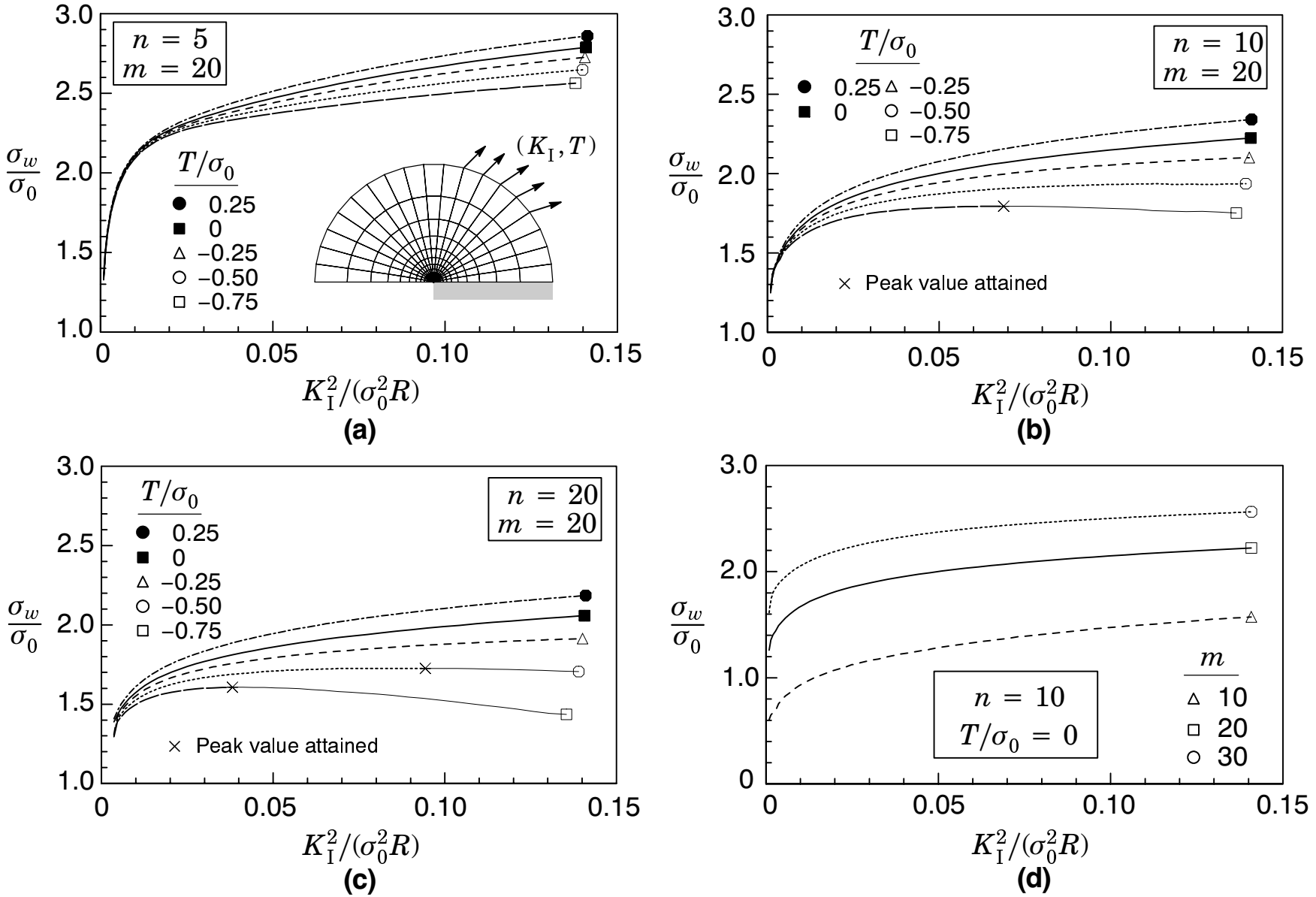


**Fig. 4.** Stationary crack analysis under SSY conditions and varying hardening properties for $E/\sigma_0 = 500$.

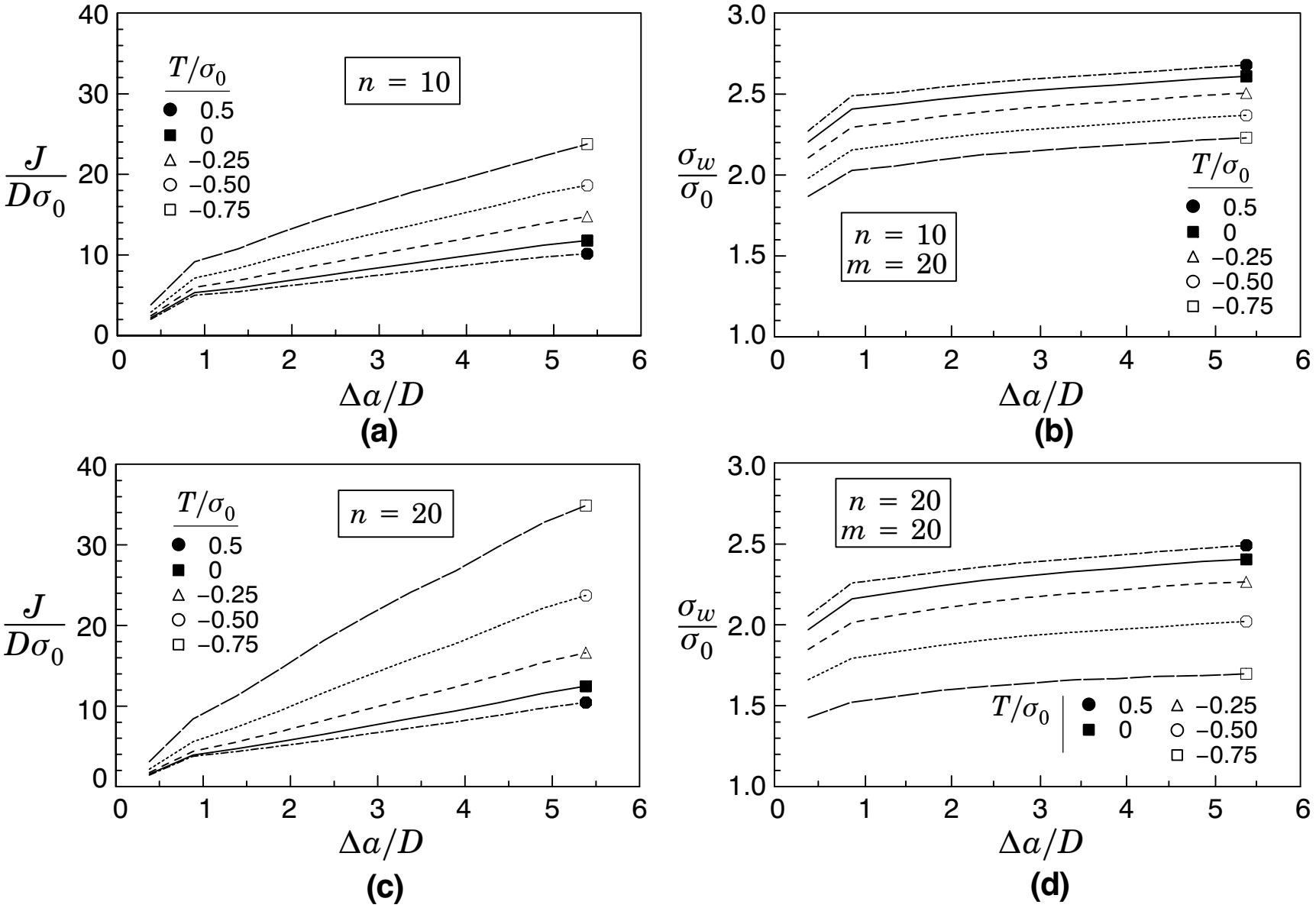


**Fig. 5.** Crack growth analyses under SSY conditions and varying hardening properties for $E/\sigma_0 = 500$ and $f_0 = 0.001$ (Weibull stress is computed using the instantaneous fracture process zone).

**Acknowledgements**

This investigation was supported by grants principally from the Scientific Foundation of the State of São Paulo (FAPESP) under Grant 98/10574-2. Access to the Cray J-90 and the SGI-Origin 200 at the High Performance Computing Center (LCCA) of the University of São Paulo is also acknowledged.

## References

1. Ruggieri, C., "A Framework to Correlate Effects of Constraint Loss and Ductile Tearing on Fracture Toughness – Part I: Probabilistic Approach," *15th Brazilian Congress of Mechanical Engineering (Cobem 99)*, Águas de Lindóia, Brazil (1999).
2. Beremin, F.M, "A Local Criterion for Cleavage Fracture of a Nuclear Pressure Vessel Steel," *Metallurgical Transactions,* Vol. 14A, pp. 2277–2287, 1983.
3. Parks, D.M., "Advances in Characterization of Elastic–Plastic Crack–Tip Fields," in *Topics in Fracture and Fatigue,* A. S. Argon, Ed., Springer Verlag, pp. 59–98, 1992.
4. Ruggieri, C. and Dodds, R. H., "A Transferability Model for Brittle Fracture Including Constraint and Ductile Tearing Effects: A Probabilistic Approach," *International Journal of Fracture*, Vol. 79, pp. 309-340, 1996.
5. Ruggieri, C. and Dodds, R. H., "Probabilistic Modeling of Brittle Fracture Including 3-D Effects on Constraint Loss and Ductile Tearing," *Journal de Physique*, Vol. 1996.
6. Ruggieri, C. and Dodds, R. H., "WSTRESS Release 1.0: Numerical Computation of Probabilistic Fracture Parameters for 3-D Cracked Solids," *BT–PNV–30(Technical Report)*, EPUSP, University of São Paulo, 1997.
7. Ruggieri, C., Dodds, R. H. and Wallin, K., "Constraints Effects on Reference Temperature, $T_0$, for Ferritic Steels in the Transition Region," *Engineering Fracture Mechanics*, Vol. 60, pp. 19-36, 1998.
8. Wallin, K. "The Scatter in $K_{Ic}$ Results," *Engineering Fracture Mechanics,* Vol. 19, pp. 1085–1093, 1984.
9. Mudry, F., 1987, "A Local Approach to Cleavage Fracture", *Nuclear Engineering and Design*, Vol. 105, pp. 65–76.
10. Minami, F., Brückner–Foit, A., Munz, D.and Trolldenier, B., "Estimation Procedure for the Weibull Parameters Used in the Local Approach," *International Journal of Fracture*, Vol. 54, pp. 197–210, 1992.
11. Gao,X., Ruggieri, C. and Dodds, R. H., "Calibration of Weibull Stress Parameters Using Fracture Toughness Data". (*Submmitted for Publication*).
12. Ruggieri, C., Gao, X. and Dodds, R. H., "Transferability of Elastic-Plastic Fracture Toughness Using the Weibull Stress Approach: Significance of Parameter Calibration". (*Submmitted for Publication*).
13. Koppenhoefer, K., Gullerud, A., Ruggieri, C., Dodds, R. and Healy, B., "WARP3D: Dynamic Nonlinear Analysis of Solids Using a Preconditioned Conjugate Gradient Software Architecture", *Structural Research Series (SRS) 596*, UILU–ENG–94–2017, University of Illinois at Urbana–Champaign, 1994.
14. Moran, B., and Shih, C.F., "A General Treatment of Crack Tip Contour Integrals", *International Journal of Fracture,* Vol. 35, pp. 295–310, 1987.
15. Larsson, S. G. and Carlsson, A. J., "Influence of Non–Singular Stress Terms and Specimen Geometry on Small Scale Yielding at Crack–Tips in Elastic–Plastic Materials", *Journal of the Mechanics and Physics of Solids*, Vol. 21, pp. 447–473, 1973.
16. Mann, N. R., Schafer, R. E. and Singpurwalla, N. D., *Methods for Statistical Analysis of Reliability and Life Data*, Jonh Wiley & Sons, New York, 1974.
17. Ruggieri, C. and Dodds, R. H., "Micromechanics and Continuum Modeling of 3-D Constraint Effects for Fracture Assessments of Structures," *15th Brazilian Congress of Mechanical Engineering (Cobem 99)*, Águas de Lindóia, Brazil (1999).
18. Ruggieri, C. and Dodds, R. H., "3-D Modeling of Mode I Crack Growth in Structural Materials," *15th Brazilian Congress of Mechanical Engineering (Cobem 99)*, Águas de Lindóia, Brazil (1999).
19. Xia, L. and Shih, C. F., "Ductile Crack Growth - I. A Numerical Study Using Computational Cells with Microstructurally-Based Length Scales," *Journal of the Mechanics and Physics of Solids*, Vol. 43, pp. 233-259, 1995.
20. Xia, L. and Shih, C. F., "Ductile Crack Growth - II. Void Nucleation and Geometry Effects on Macroscopic Fracture Behavior," *Journal of the Mechanics and Physics of Solids*, Vol. 43, pp. 1953–1981, 1995.
21. Xia, L. and Shih, C. F., "Ductile Crack Growth - III. Statistical Aspects of Cleavage Fracture After Tearing," *Journal of the Mechanics and Physics of Solids,* Vol. 44, pp. 603–639, 1996.
22. Gurson, A. L., "Continuum Theory of Ductile Rupture by Void Nucleation and Growth: Part I - Yield Criteria and Flow Rules for Porous Ductile Media," *Journal of Engineering Materials and Technology*, Vol. 99, pp. 2-15.
23. Tvergaard, V., "Material Failure by Void Growth to Coalescence," *Advances in Applied Mechanics*, Vol. 27, pp. 83-151, 1990.
24. Varias, A. G. and Shih, C. F., "Quase–Static Crack Advance Under a Range of Constraints – Steady State Fields Based on a Characteristic Length", *Journal of the Mechanics and Physiscs of Solids*, Vol. 41, pp. 835–861, 1993.
25. Dodds, R. H., Tang, M. and Anderson, T. L., "Effects of Prior Tearing on Cleavage Fracture Toughness in the Transition Region" in *Constraint Effects in Fracture, Theory and Application*, ASTM STP 1244, M. Kirk and A. Bakker, Eds., American Society for Testing and Materials, Philadelphia, Pennsylvania, 1993.
26. Williams, M.L., "On the Stress Distribution at the Base of a Stationary Crack", *Journal of Applied Mechanics,* Vol. 24, pp. 109–114, 1957.
27. Ruggieri, C. and Dodds, R. H., "Numerical Modeling of Ductile Crack Growth in 3-D Using Computational Cell Elements," *International Journal of Fracture*, Vol. 82, pp. 67-95, 1996.